

RAD: A Realistic Multi-View Benchmark for Pose-Agnostic Anomaly Detection

Kaichen Zhou^{1*}, Xinhai Chang^{2*}, Taewhan Kim^{2*}, Jiadong Zhang^{3*}, Yang Cao⁸, Chufei Peng⁵, Fangneng Zhan¹, Hao Zhao⁶, Hao Dong², Kai Ming Ting⁷, Ye Zhu⁸

Abstract—Anomaly detection is a core capability for robotic perception and industrial inspection, yet most existing benchmarks are collected under controlled conditions with fixed viewpoints and stable illumination, failing to reflect real deployment scenarios. We introduce RAD (Realistic Anomaly Detection), a robot-captured, multi-view dataset designed to stress pose variation, reflective materials, and viewpoint-dependent defect visibility. RAD covers 13 everyday object categories and four realistic defect types—scratched, missing, stained, and squeezed—captured from over 60 robot viewpoints per object under uncontrolled lighting. We benchmark a wide range of state-of-the-art approaches, including 2D feature-based methods, 3D reconstruction pipelines, and vision-language models (VLMs), under a pose-agnostic setting. Surprisingly, we find that mature 2D feature-embedding methods consistently outperform recent 3D and VLM-based approaches at the image level, while the performance gap narrows for pixel-level localization. Our analysis reveals that reflective surfaces, geometric symmetry, and sparse viewpoint coverage fundamentally limit current geometry-based and zero-shot methods. RAD establishes a challenging and realistic benchmark for robotic anomaly detection, highlighting critical open problems beyond controlled laboratory settings. The dataset and code will be released publicly to foster research in pose-agnostic, reflection-aware anomaly detection. Code and dataset could be found here: <https://github.com/kaichen-z/rad>.

I. INTRODUCTION

Anomaly detection is a fundamental capability for robotic perception and industrial inspection, enabling robots to identify defects and irregularities during manufacturing, assembly, and maintenance [1]. As vision-based inspection systems are increasingly deployed on robotic platforms, anomaly detection must operate under unconstrained viewpoints, varying illumination, and complex material properties—conditions that are rarely encountered in existing benchmarks.

Despite significant progress, most widely used anomaly detection datasets, such as MVTec AD [2] and VisA [3], are collected under controlled laboratory setups with fixed camera viewpoints, uniform backgrounds, and stable lighting. These assumptions simplify the detection problem but fail to reflect real robotic inspection scenarios, where cameras mounted on robotic arms observe objects from continuously changing poses. Even for defect-free objects, modest viewpoint changes can drastically alter appearance due to shading,

specular reflections, or partial occlusions, making pose-agnostic anomaly detection fundamentally more challenging.

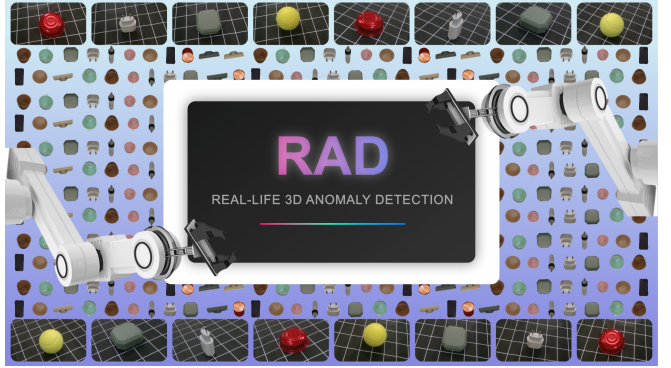


Fig. 1. **Gallery of RAD.** RAD contains 13 industrial object categories captured from 68 robot viewpoints under uncontrolled illumination, introducing variations in pose, reflectance, and geometric symmetry that pose significant challenges for existing anomaly detectors.

Recent efforts have attempted to bridge this gap by incorporating multi-view data [4], [5], 3D reconstruction [6], [7], or vision-language models (VLMs) [8]. While promising, these approaches introduce new assumptions that often break in practice. Geometry-based methods [9], [10], [11] rely on accurate pose estimation and novel-view synthesis, which are highly sensitive to reflective surfaces, geometric symmetry, and sparse view coverage. Zero-shot VLMs [8], [12], although powerful at high-level reasoning, lack pixel-level supervision and struggle to distinguish true defects from appearance changes caused by viewpoint variation. As a result, it remains unclear how existing methods perform under realistic robotic inspection conditions.

To address this gap, we introduce RAD (Realistic Anomaly Detection), a robot-captured, multi-view dataset and benchmark designed to reflect real-world inspection complexity. RAD contains 13 everyday object categories, each captured from 68 diverse robotic viewpoints under uncontrolled illumination, and includes four realistic defect types—scratched, missing, stained, and squeezed. The dataset emphasizes pose variation, reflective materials, and geometric symmetry, making anomaly detection substantially more challenging than in prior benchmarks.

Using RAD, we benchmark state-of-the-art 2D feature-based methods, 3D reconstruction pipelines, and vision-language models under a pose-agnostic setting. A key finding emerges: mature 2D feature-embedding methods consistently outperform recent 3D and VLM-based approaches

* KZ, XC, TK, and JZ contributed equally to this work. ¹ KZ and FZ are with the Massachusetts Institute of Technology. ² XC, TK, and HD are with the Peking University. ³ JZ is with the Carnegie Mellon University. ⁴ YC is with Great Bay University. ⁵ CP is with Harvard University. ⁶ HZ is with Tsinghua University. ⁷ KT is with Nanjing University. ⁸ YC and YZ is with Deakin University. Corresponding to YZ ye.zhu@ieee.org.

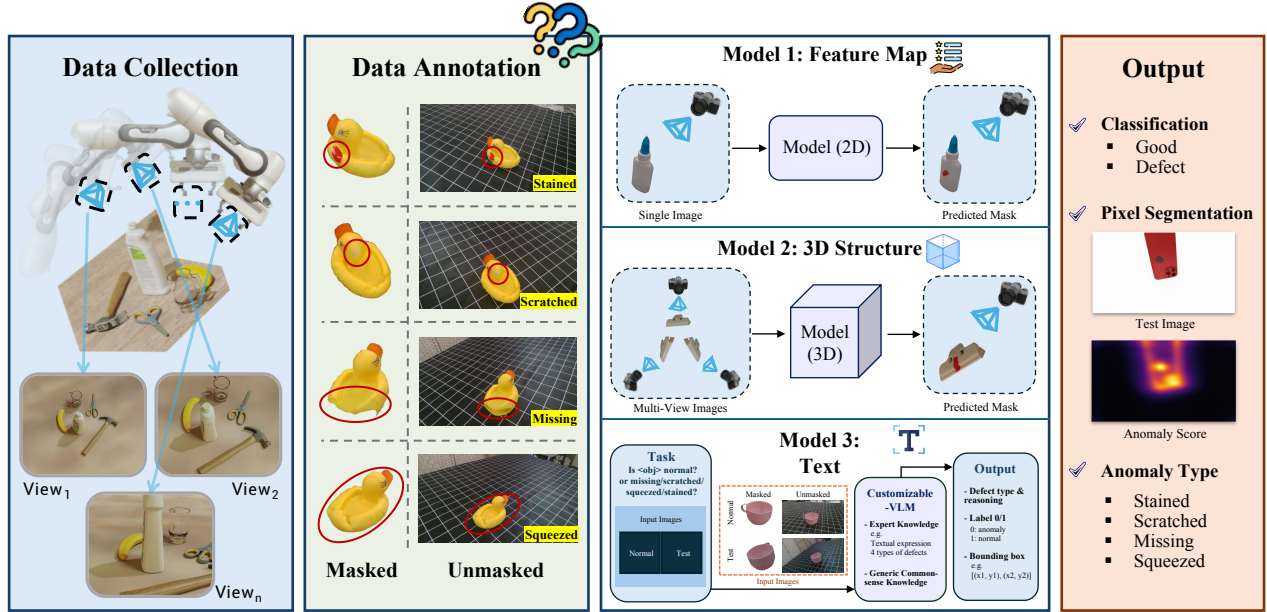


Fig. 2. **Overview of the RAD Anomaly Detection Benchmark Pipeline.** The framework integrates robotic multi-view Data Collection, fine-grained Data Annotation, and three specialized models (2D, 3D, and customizable Text-VLM) to achieve comprehensive outputs including classification, pixel segmentation, and anomaly type identification.

at the image level, despite the latter explicitly modeling geometry or semantics. While 3D methods achieve competitive pixel-level localization, their robustness is limited by pose ambiguity, reconstruction artifacts, and reflectance effects. VLMs perform poorly at both image- and pixel-level detection due to sensitivity to imaging conditions and lack of spatial supervision.

Our analysis identifies three fundamental challenges for realistic robotic inspection: reflective materials, geometric symmetry, and sparse viewpoint coverage. These results indicate that neither naïve geometry augmentation nor zero-shot VLMs are sufficient, motivating future methods that jointly reason over appearance and geometry with uncertainty awareness. Overall, RAD provides a challenging and realistic testbed for advancing pose-agnostic anomaly detection in robotics.

II. RELATED WORK

A. Anomaly Detection Datasets.

Anomaly detection is crucial for industrial automation and quality control [17]. In 2D, benchmarks like MVTec AD [2] set a standard by providing defect-free training images and diverse test anomalies. Extensions such as MVTec LOCO [18] and VisA [3] added structural/logical anomalies and high-resolution multi-instance scenes. However, these single-view RGB datasets lack 3D geometry, hindering detection of spatially or viewpoint-dependent defects.

To address this limitation, several 3D anomaly detection datasets have been proposed. MVTec 3D-AD [4] paired RGB with aligned point clouds but used a single fixed view under controlled lighting. MPDD [5] offered multi-view metal parts but limited scale. Eyecandies [13] used synthetic candy-like objects but lacks realism and multi-view support. Real 3D-AD [14] operates purely in 3D point clouds but

requires impractical scanning setups. Real-IAD [15] captures 30 objects from only five fixed angles, offering sparse pose coverage. PAD [6] introduced pose-agnostic 3D anomaly detection using toy blocks, limiting industrial relevance. SiM3D [16] bridges sim-to-real with multi-modal views but assumes perfect pose alignment.

As shown in table I, RAD is the first high-fidelity, multi-view, pose-agnostic benchmark targeting realistic robotic inspection of everyday objects. It uniquely emphasizes reflective surfaces, geometric symmetries, and viewpoint-dependent defect visibility—critical yet overlooked challenges. By capturing over 60 uncontrolled robotic viewpoints per object, RAD offers a more authentic testbed for robust, geometry-aware, pose-invariant anomaly detection.

B. Unsupervised Anomaly Detection.

Most unsupervised methods follow MVTec AD’s setup: train on normal 2D RGB images and infer pixel-wise anomaly maps. They fall into two categories: reconstruction-based [19], [20], [21], [22], [23], [24], which detect reconstruction failures, and feature embedding-based [25], [26], [27], [28], [29], [30], which flag deviations in learned feature spaces. To handle limited data, few-shot [31], [32] and zero-shot approaches [33], [34], [35], [36], [37], [38] leverage pre-trained models, while anomaly synthesis [39], [40], [41] augments training with pseudo-defects.

With MVTec 3D-AD [4], multimodal methods emerged. AST [42] uses depth only for masking, remaining 2D at core; M3AD [43] fuses RGB and point cloud features explicitly. More recently, pose-agnostic detection (PAD) [6] gained traction. OmniposeAD [7] uses Neural Radiance Fields (NeRF) [44] and iNeRF [45] for pose refinement and view synthesis. SplatPose [46] replaces NeRF with 3D Gaussian Splatting (3DGS) [47] for faster, differentiable

TABLE I

COMPARISON OF RAD AND EXISTING INDUSTRIAL ANOMALY DETECTION DATASETS. RGB, D, PC, AND NM STAND FOR RGB IMAGE, DEPTH, POINT CLOUD, AND NORMAL MAPS, RESPECTIVELY. SURFACE REPRESENTS THE OBJECTS THAT ARE TRANSPARENT OR SPECULAR.

Datasets	Representation	Type	#Class	# Normal	#Abnormal	#Shoots	View	Color	Surface	Train. Pose	Test. Pose
MVTec AD [2]	RGB	real	15	4,096	1,258	1	Single	Diverse	Specular	2D	2D
MPDD [5]	RGB	real	6	1,064	282	1	Single	Diverse	Specular	2D	2D
VisA [3]	RGB	real	12	9,621	1,200	1	Single	Diverse	Specular	2D	2D
MVTec 3D-AD [4]	RGB/D/PC	real	10	2,904	948	1	Single	Diverse	Specular	3D	2D
Eyecandies [13]	RGB/D/NM	synth	10	13,250	2,250	1	Single	Diverse	Transparency	3D	2D
Real3D-AD [14]	RGB/D/PC	real	12	652	602	360°	Multi	Diverse	Transparency	3D	2D
PAD [6]	RGB	synth	20	4,960	4,412	Around 20	Multi	Diverse	Specular	3D	2D
PAD [6]	RGB	real	10	271	490	Around 20	Multi	Diverse	Specular	3D	2D
Real-IAD [15]	RGB	real	30	99,721	51,329	5	Multi	Diverse	Specular	3D	3D
SiM3D [16]	RGB/D/PC	synth	10	5,000	1,500	20	Multi	Diverse	Specular	3D	3D
RAD (Ours)	RGB	real	13	1,224	3,063	68	Multi	Diverse	Specular	3D	3D

SE(3) pose optimization. PIAD [48] adds reflectance decomposition to 3DGS, achieving joint invariance to pose and illumination—key for reflective objects.

Concurrently, Vision-Language Models (VLMs) enable zero-shot anomaly understanding. Commercial models like Qwen [8] and GPT-4o [12] show promise in industrial contexts [49], while specialized methods [50], [51], [52], [53] use prompt engineering for competitive zero-shot performance. However, VLMs typically output only image-level classifications, lack pixel-level localization, and remain sensitive to clutter, texture details, and viewpoint changes.

III. DATASET

A. Data Acquisition

Robotic capture setup. RAD is collected using a Franka Emika Panda robotic arm equipped with an Intel RealSense D415 RGB-D camera (1280×720). Each object is captured from 68 predefined viewpoints spanning a full 360° rotation. Objects are placed at the workspace center to ensure consistent imaging geometry. Camera poses are recorded for each view; however, only RGB images are released due to real-world depth noise.

Advantages over conventional setups. Compared to multi-camera rigs or rotating scanners used in prior datasets (e.g., PAD [6], Real3D-AD [14]), the robotic arm enables dense multi-view coverage using a single sensor without object manipulation, closely reflecting practical industrial inspection scenarios while maintaining high repeatability.

Annotation protocol. Pixel-wise anomaly masks are generated by comparing defective images against corresponding normal views. Object regions are first annotated in a normal reference image, after which anomalies are manually labeled in the defective image using Adobe Photoshop, producing precise binary masks for scratches, stains, missing parts, and deformations (Fig. 3).

Anomaly types. RAD includes four realistic defect types: (1) *Scratched*—surface incisions; (2) *Missing*—removed components; (3) *Stained*—localized discoloration, and (4) *Squeezed*—mechanical deformation. Due to material rigidity, squeezed defects are excluded for binderclip, box, charger, and phonecase categories. (see Fig. 4a).

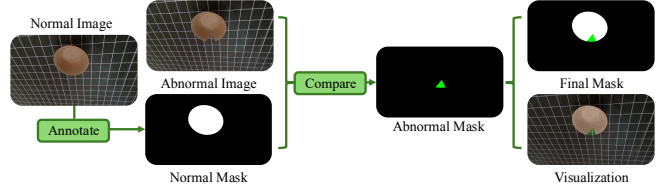


Fig. 3. **Illustration of Annotation Procedure:** This diagram illustrates the annotation process for identifying missing components. Annotations for missing parts rely on comparing defective objects with normal ones.

B. Data Statistics

RAD consists of 5,848 RGB images across 13 everyday object categories, including kitchenware, toys, and consumer items (e.g., cup, spoon, phonecase, tennis ball). Each category contains defect-free training samples and test images with up to four anomaly types. As summarized in Table II and Fig. 4, the dataset exhibits diverse geometry, material reflectance, and defect scales. Each image is accompanied by camera pose metadata, enabling research on geometry-aware and pose-agnostic anomaly detection. Overall defect distribution is balanced, with category-specific variations driven by material properties.

IV. RAD BENCHMARK

A. Task: Pose-Agnostic Anomaly Detection

In real robotic inspection, objects are observed from unknown and continuously varying viewpoints due to unconstrained robot motion. As a result, the same defect-free object can appear drastically different across views, making pose-agnostic anomaly detection essential.

The PAD [54] framework defines this task as identifying and localizing defects when the object’s pose is unknown and unconstrained. Unlike traditional anomaly detection—where training and test images are captured from fixed, aligned viewpoints—PAD requires the system to discern whether appearance differences stem from true anomalies or mere pose changes, a condition rarely avoidable in real robotic settings. Formally, let the training set be

$$R = \{(r_i, T_i)\}_{i=1}^N,$$

where each normal image r_i is paired with a known camera pose $T_i \in SE(3)$. At test time, a query image q with unknown pose T (possibly containing anomalies) is provided.

The goal is to detect and localize anomalies without any anomalous training data. PAD methods typically estimate an optimal pose \hat{T} of the query image by aligning it to a 3D model \mathcal{M} (e.g., NeRF or 3D Gaussian Splatting) trained solely on normal views:

$$\hat{T} = \arg \min_{T \in SE(3)} \mathcal{L}_{\text{align}}(q, \mathcal{R}_{\mathcal{M}}(T)), \quad (1)$$

where $\mathcal{R}_{\mathcal{M}}(T)$ renders the model from pose T ; q is the queried image and $\mathcal{L}_{\text{align}}$ is a photometric or structural loss (e.g., $L_1 + \text{SSIM}$). The anomaly score is then computed in deep feature space:

$$s(u) = \sum_{\ell} \|f^{\ell}(q)(u) - f^{\ell}(\mathcal{R}_{\mathcal{M}}(\hat{T}))(u)\|_2, \quad (2)$$

with f^{ℓ} the feature at level ℓ , u a pixel index, and $s(u)$ the pixel-wise score. Image-level scores are obtained via aggregation (e.g., max or percentile pooling).

Why this is challenging. Pose-agnostic anomaly detection is fundamentally harder than pose-aligned settings because models must distinguish true defects from appearance changes induced by viewpoint variation. This challenge is amplified by reflective materials, textureless surfaces, and geometric symmetries, which destabilize both pose estimation and appearance comparison. Sparse training views further exacerbate out-of-distribution effects at test time.

These conditions reflect real-world robotic inspection and explain why methods performing well on pose-aligned benchmarks often degrade sharply in practice—motivating the need for realistic benchmarks such as RAD.

TABLE II

DATASET STATISTICS. “TYPE” DENOTES THE NUMBER OF DISTINCT OBJECT INSTANCES PER CATEGORY. “ATTRIBUTE” DESCRIBES SURFACE APPEARANCE: *Single* = SINGLE-COLOR NON-SPECULAR, *Multi.* = MULTI-COLOR NON-SPECULAR, *Single/Specular* = SINGLE-COLOR WITH SPECULAR REFLECTIONS, *Multi./Specular* = MULTI-COLOR WITH SPECULAR REFLECTIONS. DEFECT COLUMNS: *Miss.* = MISSING, *St.* = STAINED, *Sc.* = SCRATCHED, *Sq.* = SQUEEZED.

Category	Type	Attribute	Miss.	St.	Sc.	Sq.	Normal	Total
Binderclip	2	Single	136	136	136	0	136	544
Bowl	1	Single	68	68	60	68	68	332
Box	1	Single	45	68	68	0	68	249
Can	1	Multi./Specular	41	68	4	68	68	249
Rubberduck	1	Multi.	58	60	68	68	68	322
Spraybottle	1	Single/Specular	52	62	68	68	68	318
Cup1	1	Single	68	66	61	68	68	331
Gluebottle	2	Multi./Specular	51	23	24	68	136	302
Charger	1	Multi./Specular	66	66	5	0	68	205
Cup2	3	Single	68	29	66	68	204	435
Phonecase	2	Single	68	68	68	68	136	408
Spoon	1	Single	68	66	51	68	68	321
Tennisball	1	Multi.	67	68	68	0	68	271

B. Methods

We benchmark representative anomaly detection approaches under pose-agnostic, real-world robotic inspection

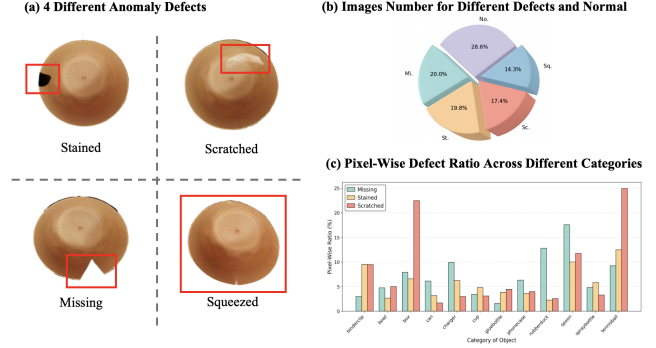


Fig. 4. **Dataset Metrics.** (a) illustrates the pixel-wise ratio within each defect across various categories. (b) shows the total number ratio of each defect in RAD. “Mi.” refers to Missing. “No.” refers to Normal. “Sq.” refers to Squeezed. “Sc.” refers to Scratched. “St.” refers to Stained. (c) shows the pixel-wise defect ratio across different categories.

settings, covering three major paradigms: 2D feature-based methods, 3D reconstruction-based methods, and vision-language model (VLM) pipelines.

2D feature-based. We evaluate eight widely used unsupervised methods operating on 2D RGB images: CFlow [30], EfficientAD [55], FastFlow [56], PaDiM [57], PatchCore [29], ReverseDistillation [58], STFPM [59], and UFlow [60]. In addition, we include three zero-shot variants based on CLIP: WinCLIP [31], AdaCLIP [34], and VCP-CLIP [35], pretrained on VisA [4]. All 2D baselines are implemented using the standard Anomalib [61] configurations to ensure reproducibility.

3D reconstruction. We benchmark SplatPose [62] and PIAD [48], which rely on recent 3D Gaussian Splatting techniques to build object-centric 3D representations from multi-view images. Given estimated camera poses, these methods render pose-aligned references and detect anomalies via geometry-consistent comparison. To better reflect real-world deployment, we use camera poses estimated by COLMAP [63], [64] on unmasked images, rather than ground-truth robotic poses.

VLM pipelines. Since off-the-shelf VLMs do not support native pixel-level anomaly localization, we evaluate Qwen2.5-VL [8] and ChatGPT-4o [12] using a three-step protocol: (1) image-level anomaly classification; (2) anomaly bounding-box prediction via prompting; (3) conversion of bounding boxes to binary masks for pixel-wise evaluation. Prompt templates are provided in the appendix. VLM results serve as complementary baselines.

C. Metric

Following prior work, we use the Area Under the Receiver Operating Characteristic Curve (AUROC) as the primary evaluation metric for both image-level anomaly classification and pixel-level segmentation, due to its robustness to class imbalance and threshold selection. AUROC is defined as:

$$\text{AUROC} = \int R_{\text{TP}} dR_{\text{FP}}, \quad (3)$$

where R_{TP} and R_{FP} denote the true positive rate and false positive rate, respectively.

TABLE III

IMAGE-WISE ROC-AUC COMPARISON ACROSS 13 OBJECT CATEGORIES ON THE RAD. BEST IN **BOLD**, RUNNER-UP UNDERLINED PER COLUMN.

Method	Type	Categories												Mean	
		binderclip	bowl	box	can	charger	cup1	cup2	gluebottle	phonecase	rubberduck	spoon	spraybottle		
Cflow	Feature	0.737	0.468	0.973	0.938	0.493	0.470	0.653	0.633	0.507	0.486	0.458	0.784	0.437	0.618
EfficientAd	Feature	0.898	0.574	0.894	0.665	0.823	0.761	0.938	0.804	<u>0.929</u>	0.717	0.806	0.882	0.963	<u>0.803</u>
Fastflow	Feature	0.802	0.815	0.871	0.758	0.681	<u>0.723</u>	0.694	0.580	0.909	0.723	0.895	0.747	<u>0.990</u>	0.786
Padim	Feature	0.694	0.630	0.495	0.690	0.431	0.530	0.443	0.524	0.625	0.534	0.572	0.546	<u>0.757</u>	0.587
Patchcore	Feature	<u>0.832</u>	0.896	<u>0.904</u>	<u>0.884</u>	0.601	0.639	<u>0.846</u>	<u>0.722</u>	0.986	0.947	0.959	<u>0.861</u>	1.000	<u>0.833</u>
ReverseDistillation	Feature	0.806	0.756	0.867	0.700	0.702	0.709	0.692	0.691	0.911	<u>0.780</u>	0.866	0.736	0.972	0.784
Stfpm	Feature	0.722	0.623	0.736	0.687	0.609	0.696	0.439	0.572	0.706	<u>0.742</u>	0.679	0.526	0.914	0.679
Uflow	Feature	0.686	0.684	0.729	0.621	0.389	0.604	0.649	0.540	0.501	0.582	0.735	0.505	0.750	0.608
WinClip	Zero-shot	0.648	0.790	0.872	0.658	0.718	0.544	0.474	0.530	0.744	0.381	0.534	0.718	0.829	0.646
AdaCLIP	Zero-shot	0.620	0.602	0.647	0.557	0.662	0.694	0.591	0.485	0.715	0.555	0.545	0.803	0.818	0.627
VCPCCLIP	Zero-shot	0.574	0.585	0.896	0.532	0.681	0.693	0.637	0.714	0.625	0.658	0.749	0.513	0.860	0.663
SplatPose	3D	0.701	0.528	0.493	0.521	0.461	0.494	0.532	0.562	0.436	0.474	0.456	0.599	0.532	0.524
PIAD	3D	0.690	0.728	0.649	0.687	0.491	0.480	0.542	0.427	0.640	0.661	0.681	0.587	0.756	0.634
Qwen-2.5	VLM	0.282	0.632	0.000	0.240	0.000	0.711	0.222	0.230	0.265	0.240	0.450	0.598	0.670	0.305
ChatGPT	VLM	0.456	0.732	0.677	0.685	0.581	0.635	0.444	0.529	0.608	0.685	0.540	0.587	0.684	0.517

For VLM-based methods, we additionally report *Type-wise AUROC*, which measures the model’s ability to distinguish among different defect categories (e.g., scratched, stained, missing, squeezed), providing finer-grained insight beyond binary anomaly detection.

V. EXPERIMENTS

A. Main Results

We conduct a systematic evaluation of three representative families of anomaly detection methods on the RAD dataset: 2D feature-based approaches, 3D reconstruction-driven techniques, and vision-language models (VLMs). Image-level and pixel-level ROC-AUC results are reported in Table IV-A and Table IV, respectively.

On image-level anomaly detection (Table IV-A), 2D feature-based methods significantly outperform both 3D reconstruction and VLM approaches. PatchCore achieves the highest average image-level AUROC of 0.833 and ranks first on seven object categories, including *phonecase*, *spoon*, and *tennisball*. EfficientAD demonstrates consistent performance across multiple categories such as *cup2* and *phonecase*, attaining the second-best average score of 0.803. In contrast, 3D methods (SplatPose and PIAD) show notably weaker results, with average AUROC scores ranging from 0.524 to 0.634. VLMs (Qwen2.5-VL and ChatGPT) perform the worst, with average AUROC below 0.52 and frequent zero scores on categories like *can*, *charger*, and *spoon*, reflecting their limited suitability for unsupervised, pose-agnostic anomaly detection.

For pixel-level segmentation (Table IV), the performance gap narrows across method types. VCPCCLIP, a zero-shot CLIP variant, leverages strong pre-trained visual representations to achieve top performance in several categories such as *box*, *cup1*, and *gluebottle*, leading all methods with an average pixel-level AUROC of 0.987. PatchCore, ReverseDistillation, and PIAD also maintain high segmentation accuracy, each exceeding 0.97 in average AUROC. Notably, although 3D methods underperform on image-level tasks, they show competitive results at the pixel level, with PIAD achieving 0.984 and SplatPose 0.977. This suggests that explicit geometric modeling supports fine-grained anomaly localization. In contrast, VLMs remain ineffective at the

pixel level, with average AUROC around 0.52, which is insufficient for industrial-grade precision.

Qualitative results (Fig. 5) further support these conclusions. 2D feature-based methods effectively detect localized texture anomalies such as scratches and stains. 3D methods suppress false positives under large pose mismatches by enforcing geometric consistency. VLMs, however, often miss true anomalies or generate incorrect detections due to background clutter or ambiguous semantics.

B. Insights and Analysis

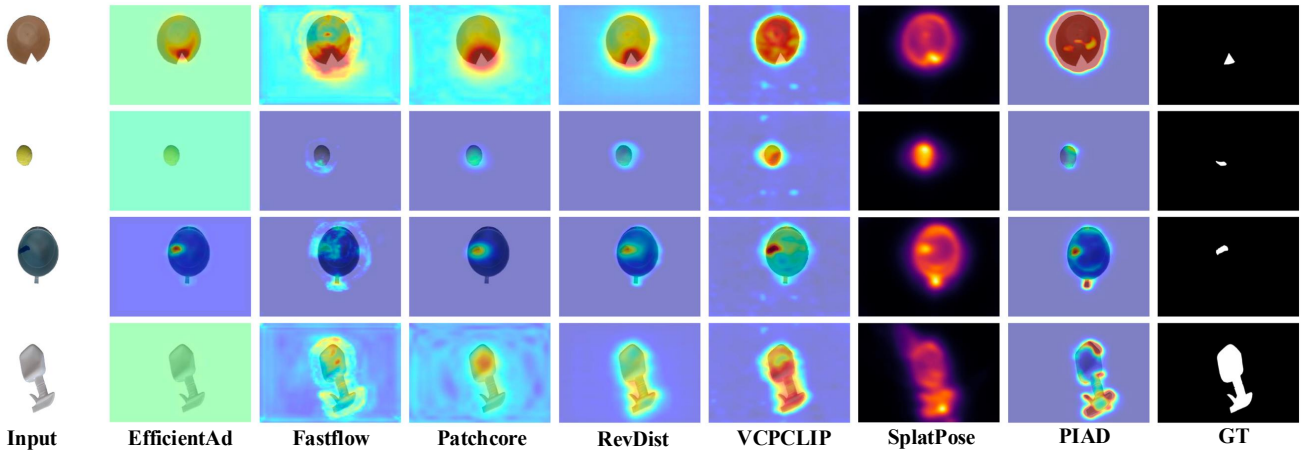
Barriers to Gains from 3D over 2D. Our experiments reveal a key observation: in realistic, pose-agnostic anomaly detection scenarios, mature 2D feature embedding methods such as PatchCore and EfficientAD substantially outperform 3D reconstruction-based approaches like SplatPose and PIAD. We attribute this to a fundamental limitation in current 3D pipelines. While neural rendering techniques such as 3D Gaussian Splatting can generate geometrically consistent reference views, they remain vulnerable to sparse training views, specular reflections, and object symmetries. Under these conditions, reconstruction artifacts are often misinterpreted as anomalies during pixel-wise comparison, which amplifies errors at both pixel and image levels. In contrast, PatchCore implicitly captures multi-view appearance and geometric variability through its memory bank of normal features, exhibiting greater robustness to minor misalignments and rendering noise.

The Capability Gap of Vision-Language Models. The consistent underperformance of VLMs highlights the difficulty of applying large-scale zero-shot models to realistic anomaly detection. Although CLIP-based zero-shot methods achieve competitive results, they lack explicit semantic guidance for anomaly interpretation. Meanwhile, despite their advanced high-level reasoning abilities, commercial VLMs such as Qwen-2.5 and GPT-4o perform even worse than random guessing on RAD. This stems from three main factors: first, the absence of pixel-level localization objectives in model pretraining; second, high sensitivity to real-world imaging conditions such as lighting and shadows; and third, an inability to distinguish genuine defects from appearance changes caused by viewpoint shifts. Furthermore, because current VLMs do not natively support pixel-level

TABLE IV

PIXEL-WISE ROC-AUC COMPARISON ACROSS 13 OBJECT CATEGORIES ON THE RAD. BEST IN **BOLD**, RUNNER-UP UNDERLINE PER COLUMN.

Method	Type	Categories												Mean
		binderclip	bowl	box	can	charger	cup1	cup2	gluebottle	phonecase	rubberduck	spoon	spraybottle	
Cflow	Feature	<u>0.994</u>	0.962	0.994	<u>0.989</u>	0.998	0.972	0.977	0.989	0.981	0.988	0.985	<u>0.973</u>	0.985
EfficientAd	Feature	0.996	<u>0.966</u>	<u>0.995</u>	0.991	0.998	0.966	0.969	0.991	0.976	0.463	0.975	0.945	0.994
Fastflow	Feature	0.956	0.816	0.977	0.945	0.952	0.781	0.903	0.915	0.942	0.901	0.986	0.912	0.989
Padim	Feature	0.993	0.950	0.990	0.988	0.996	0.974	0.969	0.946	<u>0.988</u>	0.980	0.992	0.974	0.992
Patchcore	Feature	0.991	0.952	0.994	0.988	0.996	0.968	0.976	0.929	0.991	<u>0.982</u>	<u>0.994</u>	0.985	0.996
ReverseDistillation	Feature	<u>0.994</u>	0.961	0.993	0.987	<u>0.997</u>	0.980	<u>0.980</u>	0.991	0.987	0.977	0.995	0.962	0.993
Stfpm	Feature	0.990	0.952	0.984	0.980	0.991	0.960	0.957	0.983	0.978	0.959	0.985	0.950	0.984
Uflow	Feature	0.986	0.930	0.932	0.981	0.980	0.914	0.969	0.986	0.942	0.955	0.967	0.930	0.960
WinClip	Zero-shot	0.916	0.933	0.984	0.494	0.971	0.847	0.759	0.878	0.616	0.957	0.848	0.872	0.987
AdaCLIP	Zero-shot	0.984	0.902	0.979	0.984	0.977	0.932	0.940	0.989	0.964	0.967	0.985	0.951	0.905
VCPCLIP	Zero-shot	<u>0.994</u>	0.974	0.997	<u>0.989</u>	0.996	0.984	0.984	<u>0.993</u>	0.981	0.979	0.993	0.966	<u>0.995</u>
SplatPose	3D	0.990	0.965	0.984	0.991	0.993	<u>0.983</u>	0.972	0.990	0.976	0.971	0.992	0.937	0.988
PIAD	3D	<u>0.994</u>	0.955	0.985	0.988	0.995	0.978	0.986	0.985	0.970	0.992	0.954	0.991	<u>0.984</u>
Qwen-2.5	VLM	0.525	0.573	0.636	0.507	0.514	0.505	0.517	0.502	0.531	0.520	0.517	0.524	0.669
ChatGPT	VLM	0.506	0.529	0.507	0.528	0.530	0.513	0.515	0.516	0.506	0.528	0.511	0.552	0.510

Fig. 5. **Visualization of Pixel-Wise Anomaly Detection Baselines.** The heatmap visualization illustrates the ground truth and inference results for two anomalous objects, Bowl and Spraybottle.

mask generation, bounding-box approximations introduce additional inaccuracies. These limitations indicate that VLM-based approaches are not yet ready for industrial deployment.

Impact of Material Properties and Category-Specific Challenges. Detailed analysis shows that detection performance is closely tied to object material and geometry. Categories with strong specular reflectivity or geometric symmetry exhibit significant performance degradation across all methods. This confirms the core challenges emphasized in our dataset design: reflective surfaces destabilize feature matching and pose estimation, while symmetry introduces ambiguities in pose optimization, leading to overlooked or mislocalized anomalies. These findings underscore the need for robust pose-agnostic detection systems that combine accurate 3D reconstruction—either explicit or implicit—with anomaly scoring mechanisms capable of tolerating moderate misalignment.

VI. CONCLUSION

We introduced RAD, a realistic robot-captured multi-view anomaly detection benchmark that emphasizes pose variation, reflective materials, and viewpoint-dependent visibility. Covering thirteen object categories and four defect types, RAD enables systematic evaluation of 2D feature-based methods, 3D reconstruction approaches, and vision-

language models. Our experiments show that mature 2D feature-embedding methods remain strong in pose-agnostic settings, while recent 3D and VLM-based approaches still struggle—particularly under sparse views, reflections, and symmetry—despite improved pixel-level localization. These results indicate that neither naïve geometry augmentation nor zero-shot VLMs are sufficient. Progress will require models that jointly reason over appearance and geometry with uncertainty awareness, explicitly handle reflectance and symmetry, and remain robust to sparse views and minor calibration errors. RAD provides a challenging test-bed for advancing realistic, pose-agnostic anomaly detection and will be released publicly.

REFERENCES

- [1] R. Sinha, A. Elhafsi, C. Agia, M. Foutter, E. Schmerling, and M. Pavone, “Real-time anomaly detection and reactive planning with large language models,” *arXiv preprint arXiv:2407.08735*, 2024.
- [2] P. Bergmann, M. Fauser, D. Sattlegger, and C. Steger, “Mvtec ad—a comprehensive real-world dataset for unsupervised anomaly detection,” in *Proceedings of the IEEE/CVF conference on computer vision and pattern recognition*, 2019, pp. 9592–9600.
- [3] Y. Zou, J. Jeong, L. Pemula, D. Zhang, and O. Dabir, “Spot-the-difference self-supervised pre-training for anomaly detection and segmentation,” in *European Conference on Computer Vision*. Springer, 2022, pp. 392–408.
- [4] P. Bergmann, X. Jin, D. Sattlegger, and C. Steger, “The mvtec 3d-ad dataset for unsupervised 3d anomaly detection and localization,” *arXiv preprint arXiv:2112.09045*, 2021.

[5] S. Jezek, M. Jonak, R. Burget, P. Dvorak, and M. Skotak, “Deep learning-based defect detection of metal parts: evaluating current methods in complex conditions,” in *2021 13th International congress on ultra modern telecommunications and control systems and workshops (ICUMT)*. IEEE, 2021, pp. 66–71.

[6] Q. Zhou, W. Li, L. Jiang, G. Wang, G. Zhou, S. Zhang, and H. Zhao, “Pad: A dataset and benchmark for pose-agnostic anomaly detection,” *Advances in Neural Information Processing Systems*, vol. 36, 2024.

[7] X. Chen *et al.*, “Omniposead: Pose-agnostic 3d anomaly detection with neural radiance fields,” *arXiv preprint arXiv:2404.06832*, 2024.

[8] S. Bai, K. Chen, X. Liu, J. Wang, W. Ge, and S. Song, “Qwen2.5-vl technical report,” 2025. [Online]. Available: <https://arxiv.org/abs/2502.13923>

[9] K. Park, U. Sinha, J. T. Barron, S. Bouaziz, D. B. Goldman, S. M. Seitz, and R. Martin-Brualla, “Nerfies: Deformable neural radiance fields,” in *Proceedings of the IEEE/CVF International Conference on Computer Vision*, 2021, pp. 5865–5874.

[10] K. Zhou, Y. Wang, G. Chen, X. Chang, G. Beaudouin, F. Zhan, P. P. Liang, and M. Wang, “Page-4d: Disentangled pose and geometry estimation for 4d perception,” *arXiv preprint arXiv:2510.17568*, 2025.

[11] K. Zhou, J.-X. Zhong, S. Shin, K. Lu, Y. Yang, A. Markham, and N. Trigoni, “Dynpoint: Dynamic neural point for view synthesis,” *Advances in Neural Information Processing Systems*, vol. 36, pp. 69 532–69 545, 2023.

[12] OpenAI, J. Achiam, S. Adler, S. Agarwal, L. Ahmad, I. Akkaya, and F. L. Aleman, “Gpt-4 technical report,” 2024. [Online]. Available: <https://arxiv.org/abs/2303.08774>

[13] L. Bonfiglioli, M. Toschi, D. Silvestri, N. Fioraio, and D. De Gregorio, “The eyecandies dataset for unsupervised multimodal anomaly detection and localization,” in *Proceedings of the Asian Conference on Computer Vision*, 2022, pp. 3586–3602.

[14] J. Liu, G. Xie, R. Chen, X. Li, J. Wang, Y. Liu, C. Wang, and F. Zheng, “Real3d-ad: A dataset of point cloud anomaly detection,” *Advances in Neural Information Processing Systems*, vol. 36, 2024.

[15] C. Wang, W. Zhu, B.-B. Gao, Z. Gan, J. Zhang, Z. Gu, S. Qian, M. Chen, and L. Ma, “Real-iad: A real-world multi-view dataset for benchmarking versatile industrial anomaly detection,” in *Proceedings of the IEEE/CVF Conference on Computer Vision and Pattern Recognition*, 2024, pp. 22 883–22 892.

[16] A. Costanzino, P. Zama Ramirez, L. Lella, M. Ragaglia, A. Oliva, G. Lisanti, and L. Di Stefano, “Sim3d: Single-instance multiview multimodal and multisensor 3d anomaly detection benchmark,” in *International Conference on Computer Vision (ICCV)*, 2025.

[17] J. Diers and C. Pigorsch, “A survey of methods for automated quality control based on images,” *International Journal of Computer Vision*, vol. 131, no. 10, pp. 2553–2581, 2023.

[18] P. Bergmann, K. Batzner, M. Fauser, D. Sattlegger, and C. Steger, “Beyond dents and scratches: Logical constraints in unsupervised anomaly detection and localization,” *International Journal of Computer Vision*, vol. 130, no. 4, pp. 947–969, 2022.

[19] V. Zavrtanik, M. Kristan, and D. Skočaj, “Draem-a discriminatively trained reconstruction embedding for surface anomaly detection,” in *Proceedings of the IEEE/CVF International Conference on Computer Vision*, 2021, pp. 8330–8339.

[20] D. Dehaene and P. Eline, “Anomaly localization by modeling perceptual features,” *arXiv preprint arXiv:2008.05369*, 2020.

[21] Y. Liang, J. Zhang, S. Zhao, R. Wu, Y. Liu, and S. Pan, “Omnifrequency channel-selection representations for unsupervised anomaly detection,” *IEEE Transactions on Image Processing*, 2023.

[22] Z. You, L. Cui, Y. Shen, K. Yang, X. Lu, Y. Zheng, and X. Le, “A unified model for multi-class anomaly detection,” *Advances in Neural Information Processing Systems*, vol. 35, pp. 4571–4584, 2022.

[23] J. Wyatt, A. Leach, S. M. Schmon, and C. G. Willcocks, “Anoddpmp: Anomaly detection with denoising diffusion probabilistic models using simplex noise,” in *Proceedings of the IEEE/CVF Conference on Computer Vision and Pattern Recognition*, 2022, pp. 650–656.

[24] X. Yan, H. Zhang, X. Xu, X. Hu, and P.-A. Heng, “Learning semantic context from normal samples for unsupervised anomaly detection,” in *Proceedings of the AAAI conference on artificial intelligence*, vol. 35, no. 4, 2021, pp. 3110–3118.

[25] P. Bergmann, M. Fauser, D. Sattlegger, and C. Steger, “Uninformed students: Student-teacher anomaly detection with discriminative latent embeddings,” in *Proceedings of the IEEE/CVF conference on computer vision and pattern recognition*, 2020, pp. 4183–4192.

[26] M. Salehi, N. Sadjadi, S. Baselizadeh, M. H. Rohban, and H. R. Rabiee, “Multiresolution knowledge distillation for anomaly detection,” in *Proceedings of the IEEE/CVF conference on computer vision and pattern recognition*, 2021, pp. 14 902–14 912.

[27] J. Yi and S. Yoon, “Patch svdd: Patch-level svdd for anomaly detection and segmentation,” in *Proceedings of the Asian conference on computer vision*, 2020.

[28] F. V. Massoli, F. Falchi, A. Kantarci, S. Akti, H. K. Ekenel, and G. Amato, “Mocca: Multilayer one-class classification for anomaly detection,” *IEEE transactions on neural networks and learning systems*, vol. 33, no. 6, pp. 2313–2323, 2021.

[29] K. Roth, L. Pemula, J. Zepeda, B. Schölkopf, T. Brox, and P. Gehler, “Towards total recall in industrial anomaly detection,” in *Proceedings of the IEEE/CVF Conference on Computer Vision and Pattern Recognition*, 2022, pp. 14 318–14 328.

[30] D. Gudovskiy, S. Ishizaka, and K. Kozuka, “Cflow-ad: Real-time unsupervised anomaly detection with localization via conditional normalizing flows,” in *Proceedings of the IEEE/CVF winter conference on applications of computer vision*, 2022, pp. 98–107.

[31] J. Jeong, Y. Zou, T. Kim, D. Zhang, A. Ravichandran, and O. Dabeer, “Winclip: Zero-/few-shot anomaly classification and segmentation,” in *Proceedings of the IEEE/CVF Conference on Computer Vision and Pattern Recognition*, 2023, pp. 19 606–19 616.

[32] C. Huang, H. Guan, A. Jiang, Y. Zhang, M. Spratling, and Y.-F. Wang, “Registration based few-shot anomaly detection,” in *European Conference on Computer Vision*. Springer, 2022, pp. 303–319.

[33] Q. Zhou, G. Pang, Y. Tian, S. He, and J. Chen, “Anomalyclip: Object-agnostic prompt learning for zero-shot anomaly detection,” in *The Twelfth International Conference on Learning Representations*, 2023.

[34] Y. Cao, J. Zhang, L. Frittoli, Y. Cheng, W. Shen, and G. Boracchi, “Adaclip: Adapting clip with hybrid learnable prompts for zero-shot anomaly detection,” in *European Conference on Computer Vision*, 2024.

[35] Z. Qu, X. Tao, M. Prasad, F. Shen, Z. Zhang, X. Gong, and G. Ding, “Vcp-clip: A visual context prompting model for zero-shot anomaly segmentation,” 2024. [Online]. Available: <https://arxiv.org/abs/2407.12276>

[36] W. Ma, X. Zhang, Q. Yao, F. Tang, C. Wu, Y. Li, R. Yan, Z. Jiang, and S. K. Zhou, “Aa-clip: Enhancing zero-shot anomaly detection via anomaly-aware clip,” 2025. [Online]. Available: <https://arxiv.org/abs/2503.06661>

[37] B.-B. Gao, Y. Zhou, J. Yan, Y. Cai, W. Zhang, M. Wang, J. Liu, Y. Liu, L. Wang, and C. Wang, “Adaptclip: Adapting clip for universal visual anomaly detection,” 2025. [Online]. Available: <https://arxiv.org/abs/2505.09926>

[38] Q. Fang, W. Lv, and Q. Su, “Af-clip: Zero-shot anomaly detection via anomaly-focused clip adaptation,” 2025. [Online]. Available: <https://arxiv.org/abs/2507.19949>

[39] C.-L. Li, K. Sohn, J. Yoon, and T. Pfister, “Cutpaste: Self-supervised learning for anomaly detection and localization,” in *Proceedings of the IEEE/CVF conference on computer vision and pattern recognition*, 2021, pp. 9664–9674.

[40] M. Yang, P. Wu, and H. Feng, “Memseg: A semi-supervised method for image surface defect detection using differences and commonalities,” *Engineering Applications of Artificial Intelligence*, vol. 119, p. 105835, 2023.

[41] S. Jain, G. Seth, A. Paruthi, U. Soni, and G. Kumar, “Synthetic data augmentation for surface defect detection and classification using deep learning,” *Journal of Intelligent Manufacturing*, pp. 1–14, 2022.

[42] M. Rudolph, T. Wehrbein, B. Rosenhahn, and B. Wandt, “Asymmetric student-teacher networks for industrial anomaly detection,” in *Proceedings of the IEEE/CVF winter conference on applications of computer vision*, 2023, pp. 2592–2602.

[43] Y. Wang, J. Peng, J. Zhang, R. Yi, Y. Wang, and C. Wang, “Multimodal industrial anomaly detection via hybrid fusion,” in *Proceedings of the IEEE/CVF Conference on Computer Vision and Pattern Recognition*, 2023, pp. 8032–8041.

[44] B. Mildenhall, P. P. Srinivasan, M. Tancik, J. T. Barron, R. Ramamoorthi, and R. Ng, “Nerf: Representing scenes as neural radiance fields for view synthesis,” *Communications of the ACM*, vol. 65, no. 1, pp. 99–106, 2021.

[45] L. Yen-Chen, P. Florence, J. T. Barron, A. Rodriguez, P. Isola, and T.-Y. Lin, “Inerf: Inverting neural radiance fields for pose estimation,” in *2021 IEEE/RSJ International Conference on Intelligent Robots and Systems (IROS)*. IEEE, 2021, pp. 1323–1330.

[46] S. Kim *et al.*, “Splatpose: Fast and robust pose-agnostic anomaly detection,” *arXiv preprint arXiv:2410.00713*, 2024.

[47] B. Kerbl, G. Kopanas, T. Leimkühler, and G. Drettakis, “3d gaussian splatting for real-time radiance field rendering.” *ACM Trans. Graph.*, vol. 42, no. 4, pp. 139–1, 2023.

[48] K. Yang, J. Cao, Z. Bai, Z. Su, and A. Tagliasacchi, “Piad: Pose and illumination agnostic anomaly detection,” in *Proceedings of the Computer Vision and Pattern Recognition Conference*, 2025, pp. 4734–4743.

[49] X. Jiang, J. Li, H. Deng, Y. Liu, B.-B. Gao, Y. Zhou, J. Li, C. Wang, and F. Zheng, “Mmad: The comprehensive benchmark for multimodal large language models in industrial anomaly detection,” in *The Thirteenth International Conference on Learning Representations*, 2025. [Online]. Available: <https://openreview.net/forum?id=JDjER86r8v>

[50] Z. Gu, B. Zhu, G. Zhu, Y. Chen, M. Tang, and J. Wang, “Anomalygpt: Detecting industrial anomalies using large vision-language models,” *arXiv preprint arXiv:2308.15366*, 2023.

[51] J. Xu, S.-Y. Lo, B. Safaei, V. M. Patel, and I. Dwivedi, “Towards zero-shot anomaly detection and reasoning with multimodal large language models,” in *Proceedings of the Computer Vision and Pattern Recognition Conference*, 2025, pp. 20370–20382.

[52] S. Zhao, Y. Lin, L. Han, Y. Zhao, and Y. Wei, “Omniad: Detect and understand industrial anomaly via multimodal reasoning,” 2025. [Online]. Available: <https://arxiv.org/abs/2505.22039>

[53] Y. Chao, J. Liu, J. Tang, and G. Wu, “Anomalyr1: A group-based end-to-end mllm for industrial anomaly detection,” 2025. [Online]. Available: <https://arxiv.org/abs/2504.11914>

[54] M. Kruse, M. Rudolph, D. Woiwode, and B. Rosenhahn, “Splatpose & detect: Pose-agnostic 3d anomaly detection,” in *Proceedings of the IEEE/CVF Conference on Computer Vision and Pattern Recognition (CVPR) Workshops*, June 2024, pp. 3950–3960.

[55] E. R. Chan, C. Z. Lin, M. A. Chan, K. Nagano, B. Pan, S. De Mello, O. Gallo, L. J. Guibas, J. Tremblay, S. Khamis *et al.*, “Efficient geometry-aware 3d generative adversarial networks,” in *Proceedings of the IEEE/CVF conference on computer vision and pattern recognition*, 2022, pp. 16123–16133.

[56] J. Yu, Y. Zheng, X. Wang, W. Li, Y. Wu, R. Zhao, and L. Wu, “Fastflow: Unsupervised anomaly detection and localization via 2d normalizing flows,” *arXiv preprint arXiv:2111.07677*, 2021.

[57] T. Defard, A. Setkov, A. Loesch, and R. Audigier, “Padim: a patch distribution modeling framework for anomaly detection and localization,” in *International conference on pattern recognition*. Springer, 2021, pp. 475–489.

[58] H. Deng and X. Li, “Anomaly detection via reverse distillation from one-class embedding,” in *Proceedings of the IEEE/CVF conference on computer vision and pattern recognition*, 2022, pp. 9737–9746.

[59] G. Wang, S. Han, E. Ding, and D. Huang, “Student-teacher feature pyramid matching for anomaly detection,” *arXiv preprint arXiv:2103.04257*, 2021.

[60] M. Talianian, A. Pardo, and P. Musé, “U-flow: A u-shaped normalizing flow for anomaly detection with unsupervised threshold,” *Journal of Mathematical Imaging and Vision*, vol. 66, no. 4, pp. 678–696, 2024.

[61] S. Akcay, D. Ameln, A. Vaidya, B. Lakshmanan, N. Ahuja, and U. Genc, “Anomalib: A deep learning library for anomaly detection,” in *2022 IEEE International Conference on Image Processing (ICIP)*. IEEE, 2022, pp. 1706–1710.

[62] M. Kruse, M. Rudolph, D. Woiwode, and B. Rosenhahn, “Splatpose & detect: Pose-agnostic 3d anomaly detection,” in *Proceedings of the IEEE/CVF Conference on Computer Vision and Pattern Recognition*, 2024, pp. 3950–3960.

[63] J. L. Schönberger and J.-M. Frahm, “Structure-from-motion revisited,” in *Conference on Computer Vision and Pattern Recognition (CVPR)*, 2016.

[64] J. L. Schönberger, E. Zheng, M. Pollefeys, and J.-M. Frahm, “Pixel-wise view selection for unstructured multi-view stereo,” in *European Conference on Computer Vision (ECCV)*, 2016.